

Silicon carbide coated alumina tight-ultrafiltration membrane prepared by low-pressure chemical vapor deposition for sulphate ion retention

Jan, Asif; Nijboer, Michiel; Qin, Guangze; Luiten-Olieman, Mieke; Rietveld, Luuk C.; Heijman, Sebastiaan G.J.

DOI

10.1016/j.desal.2025.119085

Publication date 2025

Document VersionFinal published version

Published in Desalination

Citation (APA)

Jan, A., Nijboér, M., Qin, G., Luiten-Olieman, M., Rietveld, L. C., & Heijman, S. G. J. (2025). Silicon carbide coated alumina tight-ultrafiltration membrane prepared by low-pressure chemical vapor deposition for sulphate ion retention. *Desalination*, *613*, Article 119085. https://doi.org/10.1016/j.desal.2025.119085

Important note

To cite this publication, please use the final published version (if applicable). Please check the document version above.

Copyright

Other than for strictly personal use, it is not permitted to download, forward or distribute the text or part of it, without the consent of the author(s) and/or copyright holder(s), unless the work is under an open content license such as Creative Commons.

Takedown policy

Please contact us and provide details if you believe this document breaches copyrights.

We will remove access to the work immediately and investigate your claim.

ELSEVIER

Contents lists available at ScienceDirect

Desalination

journal homepage: www.elsevier.com/locate/desal



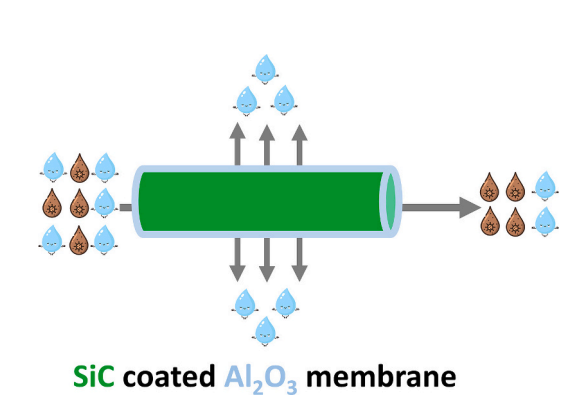
Silicon carbide coated alumina tight-ultrafiltration membrane prepared by low-pressure chemical vapor deposition for sulphate ion retention

Asif Jan^{a,*}, Michiel Nijboer^b, Guangze Qin^a, Mieke Luiten-Olieman^b, Luuk C. Rietveld^a, Sebastiaan G.J. Heijman^a

HIGHLIGHTS

- A SiC tight-UF membrane was prepared in a single-step via LP-CVD.
- The SiC tight-UF membrane had a pore size of 7 nm.
- The SiC tight-UF membrane had a highly negative surface charge.
- A sulphate ion rejection of 79 % was achieved.
- The SiC coated membrane offers a costeffective alternative to conventional membranes for ion separation.

GRAPHICAL ABSTRACT



ARTICLE INFO

Keywords: Silicon carbide Ultrafiltration Chemical vapor deposition Sulphate rejection

ABSTRACT

Sulphate $(SO_4^{2^\circ})$ is a model ion due to its negative charge and multivalent nature. Its rejection behavior serves as an indicator of the separation performance for other analogous ions in modified membranes. In literature the rejection of the $SO_4^{2^\circ}$ by negatively charged polymeric nanofiltration (NF) membranes has been studied extensively with rejection percentages of >90 %. Silicon carbide (SiC) membranes have gained attention for wastewater treatment due to their high hydrophilicity and negative charge. However, no negatively charged ceramic ultrafiltration (UF) membranes have been tested yet for $SO_4^{2^\circ}$ retention. In this study, a commercial alumina (Al₂O₃) UF membrane was converted into a highly negatively charged tight-UF membrane by coating it with SiC. This was achieved by depositing a 5 µm SiC coating in a single-step via low-pressure chemical vapor deposition (LP-CVD). LP-CVD facilitates the preparation of a SiC at much lower temperatures (700–900 °C) compared to the sol-gel methods (ca. 2100 °C), and it does not require multiple coating cycles and sintering steps to achieve the desired selective layer thickness. Subsequently, properties and performance of the as-prepared tight-UF membrane coated with SiC were evaluated. The SiC coated membrane had a highly negative charge of -70 mV at pH of 6, and a pure water permeability (PWP) of 26 L.m $^{-2}$.h $^{-1}$.bar $^{-1}$. The SiC coated membrane furthermore

^a Section of Sanitary Engineering, Department of Water Management, Faculty of Civil Engineering and Geosciences, Delft University of Technology, Stevinweg 1, 2628 CN Delft. the Netherlands

b Inorganic Membranes, Department of Chemical Engineering, MESA + Institute for Nanotechnology, University of Twente, P.O. Box 217, 7500 AE Enschede, the Netherlands

^{*} Corresponding author.

E-mail address: a.jan@tudelft.nl (A. Jan).

demonstrated a SO_4^2 rejection of 79 % despite having a large pore size of 7 nm, in comparison with the pore sizes of below 1 nm of NF membranes. These results highlight the potential of singe-step LP-CVD modification of commercial UF ceramic membranes to produce highly negatively charged SiC coated UF membranes with a high SO_4^{2-} rejection, and without a large loss of PWP normally associated with NF membranes.

1. Introduction

Industries, such as mining and the manufacturing of textiles, steel, and pharmaceuticals, produce significant quantities of wastewater [1]. These effluents contain elevated levels of various contaminants, including Na_2SO_4 and sodium chloride (NaCl) [2]. The removal of SO_4^2 ions from these wastewaters is essential to avoid environmental pollution and health hazards [3].

Membrane technology has emerged as a promising approach for wastewater treatment, offering to separate pollutants from mixtures, maintaining a high-quality permeate, and reducing operational costs [4–6]. While polymeric reverse osmosis (RO) membranes have been studied extensively and offer SO_4^2 rejection [7,8], they are afflicted by limitations such as low mechanical strength, temperature sensitivity, low flux, fouling, chemical vulnerability, and susceptibility to degradation upon chemical cleaning [9–13]. Conversely, ceramic membranes offer superior characteristics including high mechanical strength, low fouling, and stability against temperature and chemicals [14,15].

The rejection mechanism of SO_4^{2-} by membranes can involve size exclusion (steric exclusion), charge exclusion (Donnan exclusion), or a combination of both [16,17]. Steric exclusion occurs when the membranes' pore diameter is smaller than that of the SO_4^{2-} ion. Donnan exclusion whereas arises from electrostatic repulsion between the membrane's surface (meaning that the surface is negatively charged) and the negatively charged SO_4^{2-} ion.

Wadekar et al. explored the SO_4^{2-} rejection mechanisms of commercially available fully-aromatic polyamide and semi-aromatic polypiperazine, polymeric NF membranes [18]. Their findings revealed that SO_4^{2-} rejection percentages exceeded 98 %, with different mechanisms predominating in the various membrane types. The semi-aromatic polypiperazine NF membranes exhibited rejection primarily via steric exclusion, while other membranes performed through a combination of steric and Donnan exclusion mechanisms. Chong et al. modified tubular alumina microfiltration membranes into positively charged polyamide NF membranes through interfacial polymerization. In their study, a SO_4^{2-} rejection of only 65 % was observed; however, a detailed mechanistic explanation was not reported, while steric exclusion was suspected to play a role [19]. The positive charge of the membrane surface may have contributed to the observed low rejection, although further investigation may be required to confirm this.

As an alternative for the above mentioned polymeric membranes, Chen et al. tested the $SO_4^{2^-}$ rejection of a ceramic multi-channel tubular titania NF membrane [20]. The pore size of the membrane was reported to be 1.5 nm. The membrane had a low $SO_4^{2^-}$ ion rejection of 39 %, and the rejection was attributed to both steric and Donnan exclusion. In a similar study, Cha et al. measured the $SO_4^{2^-}$ rejection of a commercially-available titania NF membrane with a pore size of 0.9 nm, being ca. 60 % [21]. Although the pore size of the membrane was close to the hydrated radius of the $SO_4^{2^-}$, it was proposed that the Donnan exclusion was responsible for the $SO_4^{2^-}$ rejection. Finally, Van Gestel et al. prepared titania NF membranes by using the sol-gel dip coating procedure, and observed a $SO_4^{2^-}$ rejection of only ca. 40 % [22].

While oxide ceramics have received considerable attention [23–25], studies on carbide ceramics, such as SiC, for industrial wastewater treatment remain limited. SiC membranes prepared using the conventional sol-gel technique typically require a high-temperature sintering step (ca. $2100~^{\circ}$ C) and multiple coating and sintering cycles, thus

making the method costly [26,27]. In addition, with this method it is difficult to precisely control the pore size and selective layers' chemistry. However, the intrinsic hydrophilicity, the negative charge of SiC [28], and the low susceptibility to irreversible and reversible fouling [29], present promising attributes for SO_4^2 rejection, even with pore sizes larger than those typical of NF membranes. LP-CVD offers the advantage of depositing SiC onto membrane surface or within its pores in a single-step. The thickness of the SiC can be controlled by varying the deposition time, and structural properties can be controlled by the deposition temperature. Additionally, there is no need for a separate sintering step, which leads to significant reduction in costs [30,31]. Despite these promising characteristics of LP-CVD to produce SiC coated membranes, to the authors' knowledge, research lacks exploration into SiC coated membrane preparation by LP-CVD with ion rejection properties.

In this context, the present study focuses on the modification of commercially available tubular ${\rm Al_2O_3}$ UF membranes by depositing a coating of SiC by LP-CVD. This process transforms the ${\rm Al_2O_3}$ UF membrane into a SiC coated tight-UF membrane with different surface properties and a smaller pore size. The surface chemical composition, cross-sectional morphology, zeta potential, and pore size of the SiC coated membrane were studied. Subsequently, the performance of the SiC coated membrane was tested by measuring the PWP and ${\rm SO_4^2}$ rejection in both pure water and NaCl salt solution.

2. Materials and methods

2.1. Materials & chemical agents

Commercial single-channel tubular membranes (CoorsTek, the Netherlands) with a support and selective layer of Al_2O_3 were used for LP-CVD of SiC. The membranes had an inner diameter of 7 mm, an outer diameter of 10 mm, and were 10 cm long. As per suppliers' specifications, the mean pore size of the selective and support layers were 20 nm and 600 nm, respectively. The SiC coated tubular Al_2O_3 membranes were used for PWP, pore size measurements, scanning electron microscopy (SEM), and SO_4^{2-} rejection measurements. Flat sheet Al_2O_3 membranes (Inopor, Germany), coated with SiC under identical LP-CVD conditions, were used for zeta potential and transmission electron microscopy (TEM). The flat sheet Al_2O_3 membranes had a nominal pore size of 100 nm, a rectangular geometry of 1 cm \times 2 cm, and a thickness of 1 mm.

2.2. Low-pressure chemical vapor deposition

A hot-wall LP-CVD furnace (Tempress Systems BV, The Netherlands) was used for the deposition of SiC coating on the Al_2O_3 membrane, as described by Morana et al. [32]. The precursor Dichlorosilane (SiH $_2$ Cl $_2$) was used as the source of silicon (Si), and 5 % acetylene (C $_2$ H $_2$) in hydrogen (H $_2$) was used as source of carbon (C). Ultrapure nitrogen (N $_2$) from a liquid N $_2$ source was employed as purging gas in the system. SiC deposition was carried out at a temperature of 860 °C, a pressure of 13 Pa, and a deposition time of 40mins. During SiC deposition, the membranes were placed longitudinally to the flow of the precursor gases.

2.3. Membrane characterization and performance evaluation

The morphology of the Al₂O₃ and the SiC coated membranes was

observed by SEM (FEI Nova NanoSEM 450, USA). An energy dispersive x-ray (EDX) analyzer coupled with SEM was used to determine the Si atomic percentage. Sample preparation for SEM involved breaking the membranes with a hammer to obtain a relatively flat specimen which was afterwards sputter coated with gold to increase sample conductivity to achieve clear images.

The thickness and chemical composition of the SiC coating was studied by FEI cubed titan Cs-corrected 80-300 kV TEM. Elemental mapping in scanning transmission electron microscopy (STEM) mode was performed using the super-X in the ChemiSTEM $^{\rm TM}$ configuration. In STEM mode, a small electron beam scans the specimen. For each beam position the diffracted electrons are collected on a ring detector, thus forming an annular dark field (ADF) image after the complete area is scanned. At the same time, an EDX spectrum is collected for each beam position, and elemental maps are obtained.

Pore size measurements were performed by Micromeritics Mercury Intrusion Porosimetry (MIP). In the standard MIP test, mercury is forced to penetrate into the pore system of a specimen by increasing the applied pressure. Assuming that the pores are cylindrical in shape, the correlation between the applied pressure P (MPa) and the pore diameter d (μ m) can then be described by the Washburn equation [33]:

$$d = (-4.\gamma Hg.\cos\theta)/P$$

where γ_{Hg} (0.48 N/m) is the surface tension of the mercury [34]; θ (140°) is the contact angle between mercury and the pore wall [35].

The zeta potential was estimated on the SiC coated ${\rm Al_2O_3}$ flat-sheet membrane using an electrokinetic analyzer (SurPASS, Anton Paar, Graz, Austria). The instrument measures the streaming current coefficient, and the Helmholtz–Smoluchowski equation was then used for the calculation of the zeta potential of the membrane. The isoelectric point (IEP) was measured in a titration system, encompassing a pH range of 3 to 10.

The Debye length for feed solutions of various ionic strengths was calculated using the following equation [36]:

$$k^{-1} = \left(\frac{\varepsilon_0 \varepsilon_r k_B T}{2000 N_A e^2 I}\right)$$

where ε_0 = vacuum permittivity (8.85 × 10^{-12} C V⁻¹ m⁻¹), ε_r = relative permittivity of the background solution (80 for water at 20 °C), k_B = Boltzmann constant (1.38 × 10^{-23} JK⁻¹); T = absolute temperature (K); N_A = Avogadro number (6.0 × 10^{23} mol⁻¹); e = elementary charge (1.6 × 10^{-19} C); I = ionic strength (mol L⁻¹).

For membrane performance evaluation, Na₂SO₄ and NaCl salts were purchased from Sigma-Aldrich Chemicals (the Netherlands). Feed solutions of various concentrations were prepared with deionized (DI) water. The PWP and SO_4^{2-} ion rejection by the SiC coated membrane was measured under constant flux in an in-house built cross-flow filtration setup for tubular membranes, as described by Jan et al. [30], using DI water and NaCl salt solution. The PWP of the membranes was calculated by dividing the pure water flux by transmembrane pressure. The concentration of SO_4^{2-} in the feed and permeate samples was determined by ion chromatography (Metrohm AG, Switzerland). Before ion chromatography, the samples were filtered with a 0.45 μ m filter and diluted according to the measurement range of the instrument.

3. Results and discussion

3.1. Structural characteristics of the SiC coated Al₂O₃ selective layer

3.1.1. Morphological evolution

Surface properties of the pristine Al₂O₃ membrane, such as defects and inhomogeneities, can influence the properties and performance of any subsequently deposited coating [37]. And, given that commercially available tubular Al₂O₃ membranes are not completely defect-free [38],

an Al₂O₃ membrane with minimal inhomogeneities was selected for the coating of SiC. To identify such a membrane, the PWPs of various Al₂O₃ membranes were first measured. Membranes exhibiting similar PWP values, indicative of comparable pore structures and minimal defects, were then chosen for subsequent SiC coating to ensure consistency in performance across the selected membranes. Fig. 1 (a & c) shows the surface and cross-sectional morphologies of the Al₂O₃ membrane. In Fig. 1c, it can be observed that the Al₂O₃ membrane had an asymmetric structure comprising of a macroporous support and mesoporous selective layer with a nominal pore size of 20 nm. However, the actual pore size was different from the nominal pore size and it was measured to be 13 nm by MIP (Fig. S1). Additionally, non-homogeneous domains in the form of larger grains and pores can also be observed on the membranes' surface (Fig. 1a). In comparison, LP-CVD modification of the Al₂O₃ membrane resulted in a homogeneous SiC coating on the Al₂O₃ selective layer of the membrane, see Fig. 1b (also Fig. S2). Thus, the SiC coated Al₂O₃ selective layer could function as the new selective layer.

The PWP of a membrane is dependent on the total resistance of the support and selective layers [16]. It has been reported that the experimental hydraulic resistance of the support and selective layer can be much larger than the combined theoretical resistances of the two. The increased resistance is due to the presence of transitionary boundary layers at the interface of a macroporous support and a mesoporous/ microporous selective layer [39]. Therefore, LP-CVD conditions, i.e. temperature and pressure, must be tuned accurately to control the thickness of the coating so that the interface of selective layer and support layer remains unmodified. Moreover, the growth rate of the coating is not uniform along the axial direction of the LP-CVD furnace. The growth rate at the inlet of the furnace is high and decreases along the length of the furnace [40]. This was also validated by our observations. The SiC deposition on the Al₂O₃ membrane at the inlet of the furnace resulted in a gradient SiC coating thickness, and the SiC coating also penetrated beyond the interface of selective layer and support into the bulk of the material (Fig. S3). Therefore, the LP-CVD of the SiC was carried out further away from the inlet of the furnace and the resultant SiC coating did not penetrate into the bulk of the support, and had a constant thickness across the length of the membrane (Fig. 1d). Furthermore, in LP-CVD, the growth of the deposited material has two main aspects: (a) longitudinal growth; and (b) radial growth [41]. These affect both the selectivity and PWP due to change of effective pore size of membrane (pore size measurements will be discussed in the subsequent section). Therefore, to measure the thickness of the SiC coating, i.e. growth in longitudinal direction, a line-scan along the cross-section of the membrane was conducted via SEM-EDX (Fig. S4). The SiC coating did penetrate ca. 5 μm into the Al₂O₃ selective layer of the membrane.

3.1.2. Radial growth of SiC and effective change in pore size of membrane The radial growth of the SiC coating was analyzed by TEM and elemental mapping was conducted in the STEM mode to calculate the atomic percentages of Si and C respectively. It can be seen that the Al₂O₃ particles were completely shielded by the SiC coating (Fig. 2a-d). The radial thickness of the SiC coating was measured to be ca. 12 nm. (Fig. 2f). Additionally, the atomic percentages of Si and C were measured at area-1. Area-1 is shown in the marked circle in Fig. 2e, and the respective enlarged image is shown in Fig. 2f. Both Si and C were present in equal atomic percentages (Fig. 2g). Oxygen was also detected in the SiC coating, which can be attributed to the presence of hydroxyl (—OH) groups on the surface. These —OH groups are responsible for the negative charge and hydrophilic properties of SiC coating.

The pore size of SiC coated membrane, determined via MIP, is presented in Fig. 3. During MIP analysis, mercury initially intrudes the macropores due to the relatively low pressure required for penetration. As shown in Fig. 3a, the mean macropore size of the SiC coated membrane was found to be 650 nm. With increasing pressure, mercury progressively intrudes mesopores and micropores until the available pore volume is saturated. However, a limitation of MIP is its reduced

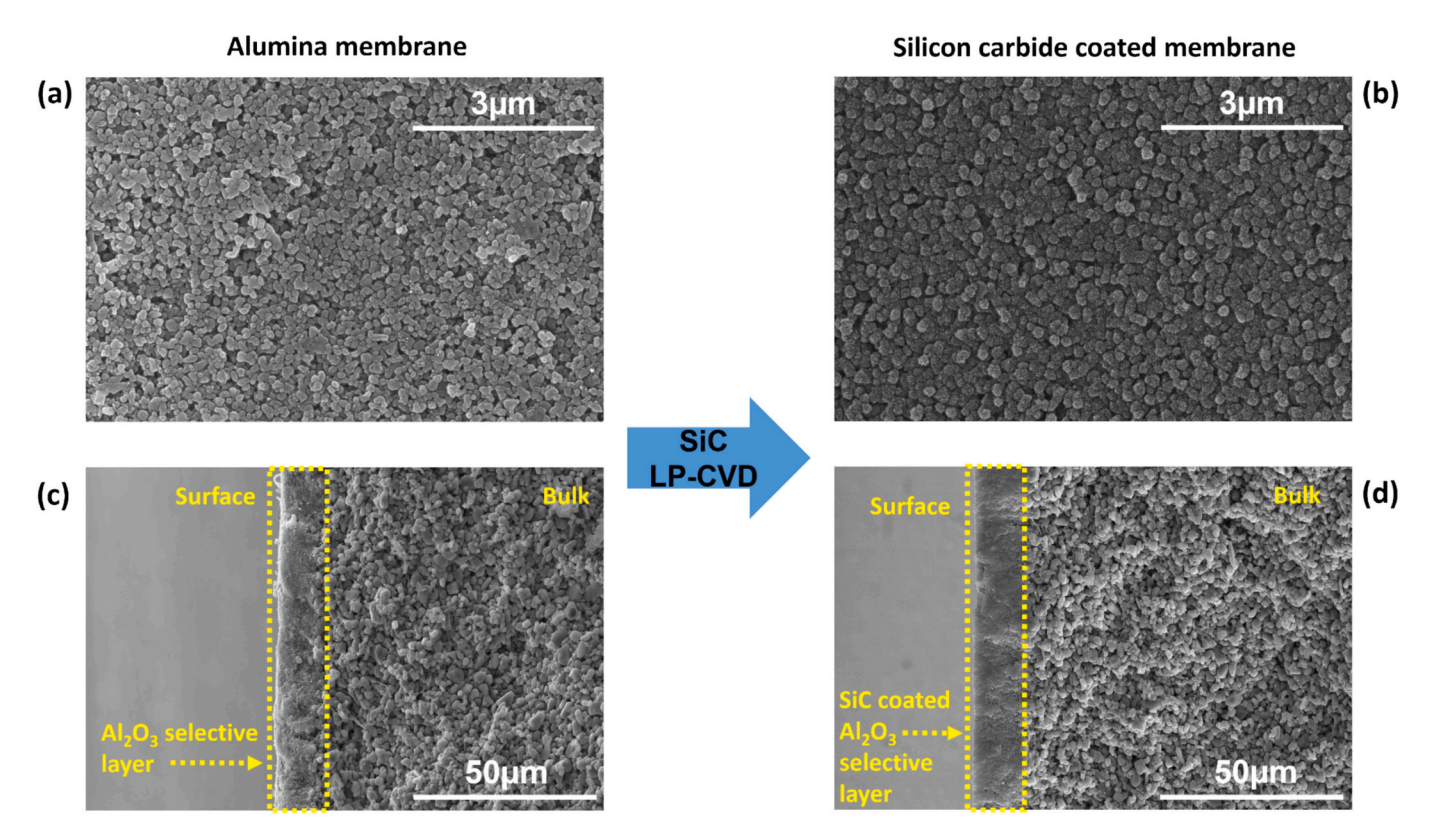


Fig. 1. Surface morphology of alumina and silicon carbide membranes (a-b); cross-sectional morphology of alumina and silicon carbide membranes (c-d).

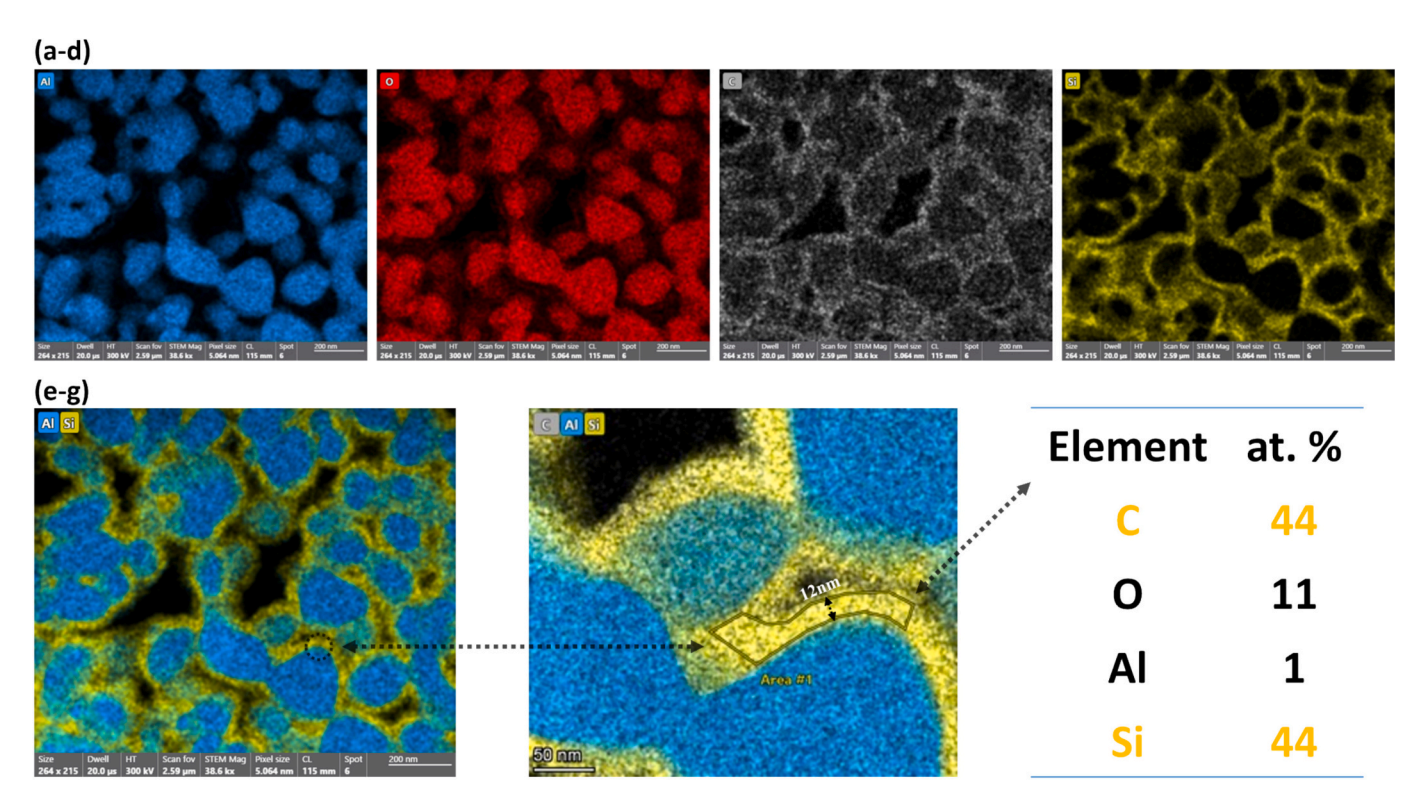
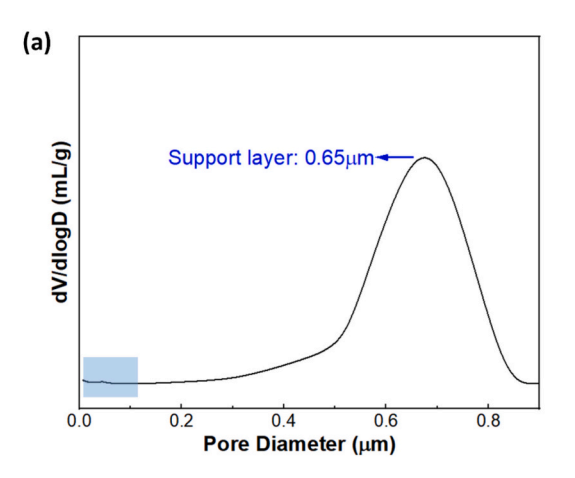


Fig. 2. STEM elemental mapping of silicon carbide selective layer (a-f); elemental composition of silicon carbide selective layer (g).

sensitivity to the pore size distribution of asymmetric membranes. Specifically, the dominant contribution of the macroporous support layer to the overall intrusion data often masks the influence of the selective layer, which has a significantly lower pore volume [42]. This

limitation is evident in the present study, as only a minimal volume of mercury was intruded into the SiC coated $\rm Al_2O_3$ selective layer, resulting in an estimated mean pore size of 7 nm (Fig. 3b).



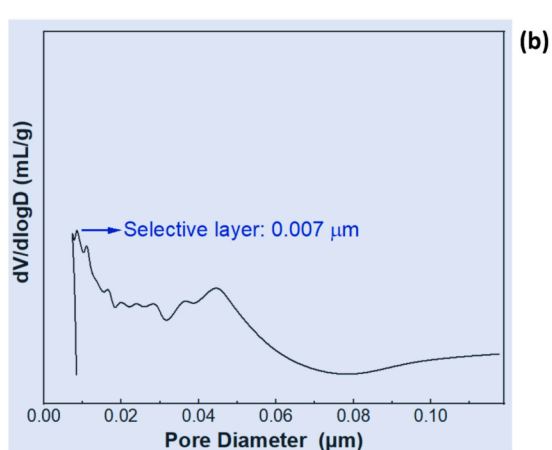


Fig. 3. Pore size of silicon carbide membrane as measured by mercury intrusion porosimetry.

3.2. SiC coated membrane properties: water permeability and zeta potential

3.2.1. Pure water permeability

The PWP of the Al_2O_3 membrane was ca. 277 L.m $^{-2}$.h $^{-1}$.bar $^{-1}$, see Fig. 4a. After deposition of SiC for 40mins, the PWP dropped to 26 L. m $^{-2}$.h $^{-1}$.bar $^{-1}$. It can be seen in Table 1 that the PWP of SiC coated membrane is high in comparison with other ceramic membranes prepared by sol-gel methods. For instance, sol-gel-based titania membranes typically exhibit PWPs ranging from 1.4 to 7 L.m $^{-2}$.h $^{-1}$.bar $^{-1}$, depending on their preparation parameters and microstructure. The high PWP of the SiC membrane can be attributed to the inherent hydrophilicity of the SiC [29], and LP-CVD process which minimizes additional pore constriction while enhancing surface properties. Additional SiC coated membranes were also prepared by extending the deposition time to 45mins. However, no PWP was observed, and it is suspected that it is due to complete pore clogging of the Al_2O_3 membranes by SiC.

3.2.2. Zeta potential

The zeta potential, also known as electrokinetic potential, is the consequential potential difference that is created between different regions of different charge densities in direction perpendicular to the pore wall. It is measured between the imaginary shear/slipping plane of electrical double layer and electrolyte [43].

The zeta potential of the SiC coated membrane remained negative across the pH range of $3{\text -}10$ and became highly negative at pH values

above 4 (Fig. 4b). This aligns with the observations reported in the literature for other SiC membranes. Studies have shown that SiC coated membranes prepared by LP-CVD consistently display negative zeta potential which reflects the distinct surface chemistry and hydrophilicity of SiC [14,31]. Full SiC membranes used in water treatment applications have demonstrated zeta potentials of -20 to -40 mV at pH 7 [44], facilitating the rejection of negatively charged solutes and mitigating fouling. In contrast, the uncoated $\mathrm{Al}_2\mathrm{O}_3$ membrane exhibited a positive charge at pH <6, transitioning to a negative charge at pH >6. Furthermore, membranes based on $\mathrm{Al}_2\mathrm{O}_3$ and titania typically exhibit an isoelectric point (IEP) between pH 5–7, where the surface charge is zero. This highlights the advantages of SiC in applications requiring treatment of anionic feeds.

3.3. SiC coated membrane rejection properties

3.3.1. Sulphate ion rejection in deionized water

Fig. 5a shows the SO_4^{2-} rejection of the SiC coated membrane as a function of increasing Na_2SO_4 feed concentration. It can be seen that the SiC coated membrane exhibited the highest SO_4^{2-} rejection of 79 % for 2 mM Na_2SO_4 feed solution. Table 1 shows that the SO_4^{2-} rejection of the SiC coated membrane is high in comparison with other ceramic nanofiltration membranes reported in literature [19–21,45–48]. However, increasing the Na_2SO_4 feed concentration to 20 mM led to a decrease of SO_4^{2-} rejection to 34 %.

The decrease of the rejection at higher feed concentrations can be attributed to the increased ionic strength of the solution which lowers

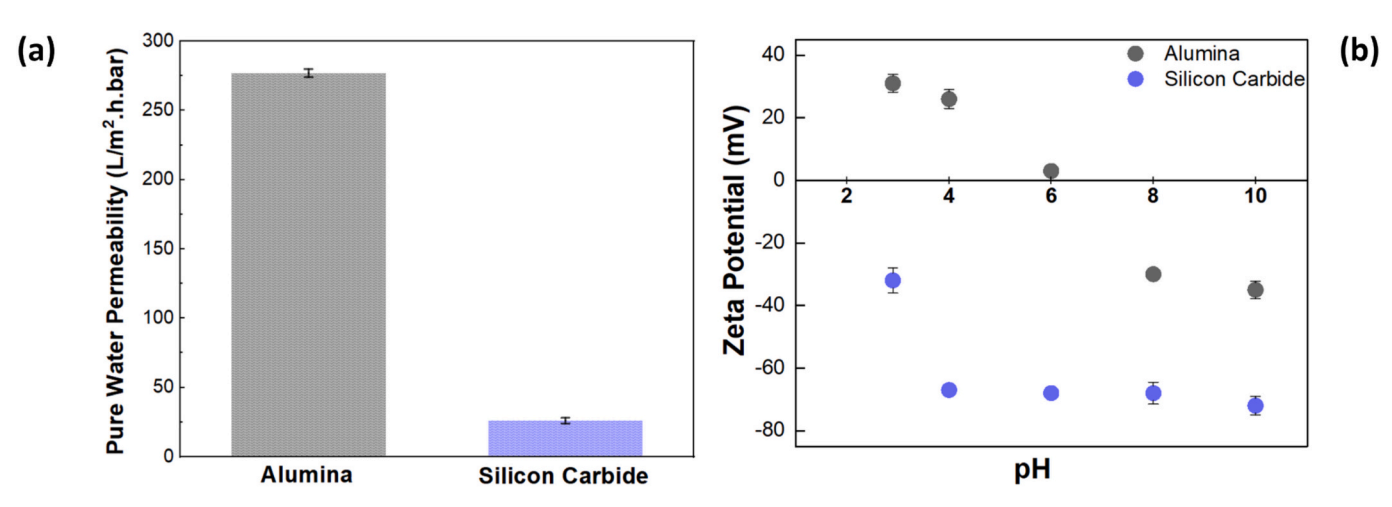


Fig. 4. Pure water permeability of membranes calculated by pure water flux and transmembrane pressure (a); zeta potential of membranes (b).

Table 1Comparison of sulphate rejection of silicon carbide membrane with membranes reported in literature.

Selective layer	Preparation method	PWP ($L.m^{-2}.h^{-1}.bar^{-1}$)	Na ₂ SO ₄ feed concentration (mM)	$\mathrm{SO_4^{-2}}$ rejection (%)	Reference
Titania	Sol-gel	_	7	39	[20]
Titania	Sol-gel	-	2	60	[21]
Titania	Sol-gel	7	100	36	[45]
Polyethersulfone	_	5	25	55	[46]
Zirconia/alumina ^a	_	-	10	70	[47]
Titania	Sol-gel	1.4	_	68	[48]
Silicon carbide	LP-CVD	26	2	<i>7</i> 9	This work

^a Both selective layers were tested for sulphate rejection, and same performance was obtained.

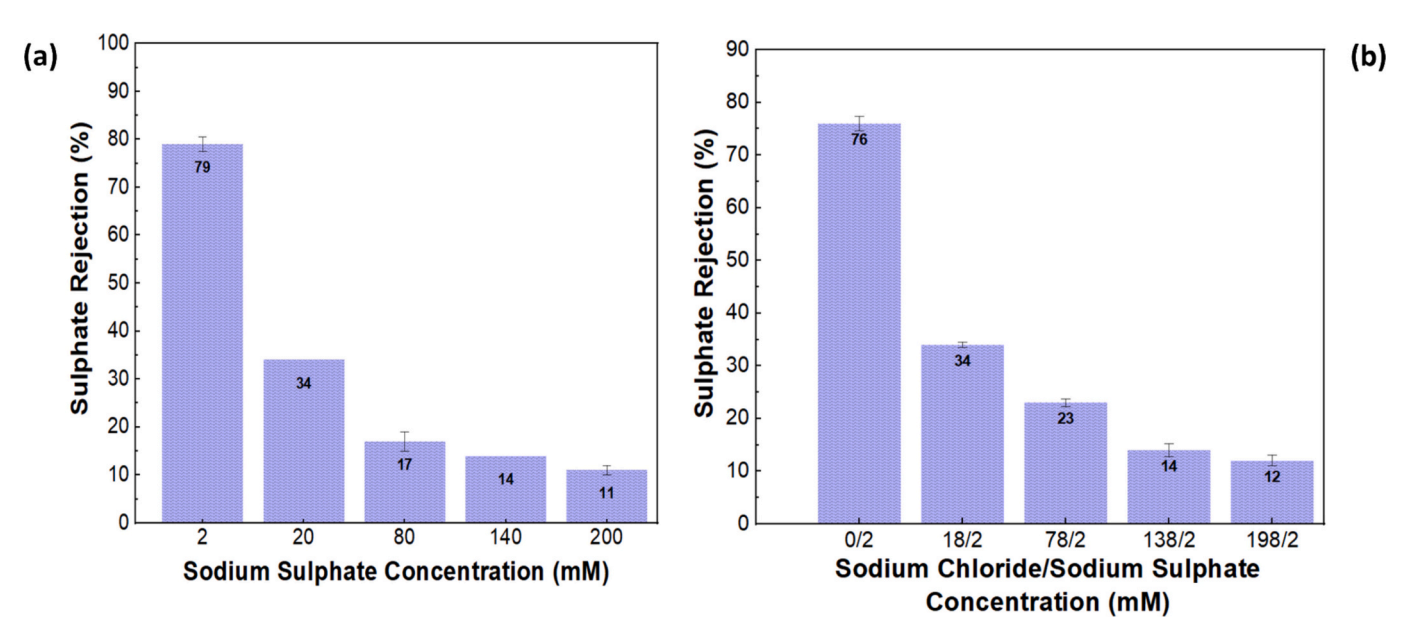


Fig. 5. Sulphate rejection of silicon carbide membrane with increasing Na₂SO₄ feed concentration (a); and mixed (NaCl and Na₂SO₄) feed solution (b).

the membranes' zeta potential [16,49]. Higher ionic strength increases the counter-ion concentration near the membrane surface, either partially or fully compensating the surface charge of membrane. This process causes a reduction in the Debye length, thereby weakening electrostatic interactions [16]. As shown in Table 2, the Debye length decreased with increasing feed ionic strength, leading to a lower zeta potential and a diminished electrostatic effect on co-ion transport through the membrane. These findings are consistent with the observed trends in SO_4^2 rejection for the SiC coated membrane.

3.3.2. Influence of mixed Na₂SO₄ and NaCl feed on sulphate ion rejection

To obtain more insights on the rejection mechanism, SO_4^{2-} rejection was also measured by using a mixed feed of NaCl and Na₂SO₄ (Fig. 5b). The Na₂SO₄ concentration was fixed at 2 mM and the NaCl concentration was varied, to correlate change in the electrical double layer with SO_4^{2-} rejection by the SiC coated membrane. For 2 mM Na₂SO₄ concentration without any NaCl, a SO_4^{2-} rejection of ca. 76 % was observed, which is consistent with the previous observations. With increasing NaCl

Table 2Debye length calculated for feed solutions of various ionic strengths.

Ionic strength (mM)	Debye length (nm)		
2	6.82		
20	2.16		
80	1.08		
140	0.82		
200	0.68		

concentration, a decreasing trend in SO₄² rejection was observed (Fig. 5b). This stems from the fact that a high concentration of sodium (Na⁺) counter-ions will compress the electrical double layer and the zeta potential of the SiC coated membrane. Nicolini et al. measured the SO_4^2 rejection of a Na₂SO₄ solution by a commercially available negatively charged polyethersulphone (NP010) membrane with an average pore radius of 1.29 nm [46]. The SO₄²⁻ rejection was ca. 55 %, and it was concluded that the increased concentration of counter-ions at the membranes' surface reduces the SO₄²⁻ (co-ion) rejection. Similarly, Caltran et al. observed that the SO₄² rejection of a mixed NaCl/Na₂SO₄ feed solution by commercially available titania membrane with a mean pore size of 0.9 nm was only 36 % [45]. They concluded that the Donnan effect is responsible for the retention and suspected that the low rejection was due to low negative zeta potential of the membrane. In the present study the SO_4^2 rejection by the SiC coated membrane for a mixed 2 mM Na₂SO₄ and 18 mM NaCl feed solution decreased to 34 %, and further increasing the NaCl concentration, while keeping Na₂SO₄ concentration fixed, led to an even more drastic decrease of SO₄² rejection.

According to Donnan exclusion principle, charged ceramic membranes can effectively repel co-ions and attract counter-ions, enabling the exclusion of ionic species whose hydrated species are much smaller than the nominal pore diameter of the membrane. The strength of this electrostatic exclusion, however, depends critically on the ratio between the pore radius and the Debye length of the electrical double layer [50]. A schematic of membrane pore size and Debye length as a function of feed ionic strength is shown in Fig. 6. At 2 mM feed ionic strength, the Debye length is calculated to be 6.82 nm (Table 2), leading to an overlap of diffuse double layer within the membrane pores. Under these

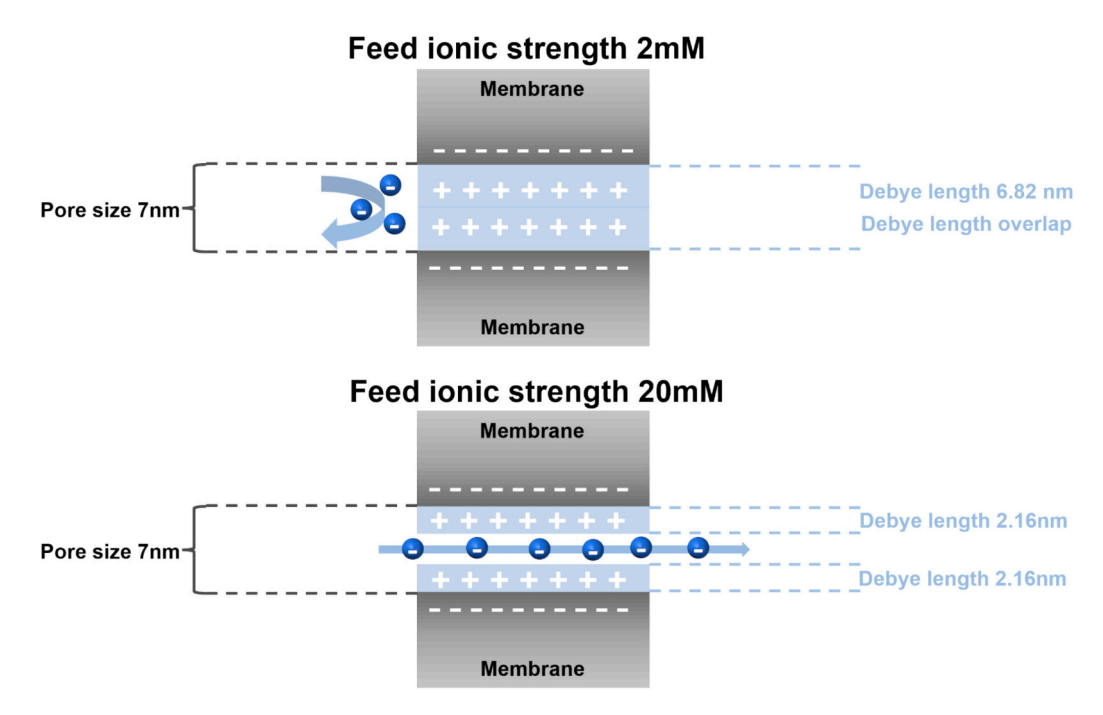


Fig. 6. Schematic of SiC coated membrane pore size and Debye length as a function of feed ionic strength.

conditions, SO_4^{2-} ions concentration is depleted in the pore interior due to the overlap of diffuse double layers. Counter ions are in excess in the diffuse double layer and the co-ions are decreased in concentration in the diffuse double layer of a negative surface. Conversely, at 20 mM feed ionic strength, the Debye length is reduced to 2.16 nm (Table 2), and thus preventing diffuse layer overlap within the pores. Consequentially, allowing co-ions (SO_4^{2-}) to penetrate the pores more freely, thus leading to lower rejection. Notably, despite having a relatively large pore size of 7 nm, the highly negatively charged SiC coated membrane effectively rejected SO_4^{2-} ions which possess a hydrated radius of 3.79 Å [51].

4. Conclusions

An Al_2O_3 UF membrane was successfully converted into a SiC tight-UF membrane in a single-step via coating with LP-CVD. The deposition conditions were optimized to form a SiC coating fully encapsulating the Al_2O_3 selective layer. Notably, the LP-CVD method eliminated the need for high temperature sintering step (ca. 2100 °C) typically required in sol-gel based SiC membrane fabrication, offering a potentially more cost-effective manufacturing route.

SEM analysis revealed that the longitudinal thickness of the SiC coating in the selective layer was 5 μm , while STEM analysis confirmed a radial thickness of only 12 nm. These deposition characteristics resulted in a membrane with a mean pore size of 7 nm. Zeta potential measurements indicated a highly negative surface charge, leading to a SO_4^2 rejection of 79 % at low feed ionic strengths, despite the membranes' relatively large pore size compared to SO_4^2 ions (size of the ion only 10 % of the pore size). However, increasing the ionic strength of both single and mixed salt solutions led to a decline in SO_4^2 rejection, highlighting the dominant role of electrostatic interactions in the separation process. These findings confirm that both pore size and Donnan exclusion govern the SO_4^2 rejection, with higher ionic strengths suppressing the electrostatic repulsion due to double layer compression.

The present study demonstrates the potential of LP-CVD derived SiC coated membranes for selective ion separation and provides insights into the interplay between membrane charge, pore structure, and feedwater chemistry, which are critical for designing efficient ceramic membranes for water purification applications.

CRediT authorship contribution statement

Asif Jan and Sebastiaan G.J. Heijman contributed to the conception of the study. Asif Jan and Sebastiaan G.J. Heijman contributed to the design of the study, which was approved by Michiel Nijboer, and Mieke Luiten-Olieman, and Luuk C. Rietveld. Asif Jan performed the majority of experiments, whereas zeta potential experiments were performed by Guangze Qin. Asif Jan wrote the original draft, which was reviewed by Michiel Nijboer, Sebastiaan G.J. Heijman, Luuk C. Rietveld, Mieke Luiten-Olieman and Guangze Qin. All authors have read and agreed to the published version of the manuscript.

Funding

This publication is part of the project "Waste to Feed; Sustainable treatment of challenging industrial (waste)streams with robust silicon carbide nano- or tight-ultrafiltration membranes (SUSSIC)" with project number 18474 of the Open Technology research program which is partly financed by the Dutch Research Council (NWO).

Declaration of competing interest

The authors declare that they have no known competing financial interests or personal relationships that could have appeared to influence the work reported in this paper.

Acknowledgements

For the Titan TEM results, we acknowledge support from the Kavli Institute of Nanoscience, Delft University of Technology, and the Netherlands Electron Microscopy Infrastructure (NEMI), project number 184.034.014, part of the National Roadmap and financed by the Dutch Research Council (NWO).

Appendix A. Supplementary data

Supplementary data to this article can be found online at https://doi.org/10.1016/j.desal.2025.119085.

Data availability

The authors do not have permission to share data.

References

- [1] A. Chatla, I.W. Almanassra, A. Abushawish, T. Laoui, H. Alawadhi, M.A. Atieh, N. Ghaffour, Sulphate removal from aqueous solutions: state-of-the-art technologies and future research trends, Desalination 558 (2023) 116615, https://doi.org/10.1016/j.desal.2023.116615.
- [2] W.A.M. Fernando, I.M.S.K. Ilankoon, T.H. Syed, M. Yellishetty, Challenges and opportunities in the removal of sulphate ions in contaminated mine water: a review, Miner. Eng. 117 (2018) 74–90, https://doi.org/10.1016/j.mineng.2017.12.004.
- [3] J.R. Werber, C.O. Osuji, M. Elimelech, Materials for next-generation desalination and water purification membranes, Nat. Rev. Mater. 1 (5) (2016) 16018, https:// doi.org/10.1038/natrevmats.2016.18.
- [4] E. Eray, V.M. Candelario, V. Boffa, Ceramic processing of silicon carbide membranes with the aid of aluminum nitrate nonahydrate: preparation, characterization, and performance, Membranes (Basel) 11 (9) (2021), https://doi. org/10.3390/membranes11090714.
- [5] A. Farsi, S.H. Jensen, P. Roslev, V. Boffa, M.L. Christensen, Inorganic membranes for the recovery of effluent from municipal wastewater treatment plants, Ind. Eng. Chem. Res. 54 (13) (2015) 3462–3472, https://doi.org/10.1021/acs.iecr.5b00064.
- [6] C. Reith, B. Birkenhead, Membranes enabling the affordable and cost effective reuse of wastewater as an alternative water source, Desalination 117 (1) (1998) 203–209, https://doi.org/10.1016/S0011-9164(98)00097-6.
- [7] S.S. Wadekar, Y. Wang, O.R. Lokare, R.D. Vidic, Influence of chemical cleaning on physicochemical characteristics and ion rejection by thin film composite nanofiltration membranes, Environ. Sci. Technol. 53 (17) (2019) 10166–10176, https://doi.org/10.1021/acs.est.9b02738.
- [8] Y. Wang, S. Zhao, Z. Zha, Z. Wang, J. Wang, Host-guest nanofiltration membranes having amino-complexed cucurbituril supramolecular channel for monovalent/ divalent salts separation, Desalination 527 (2022) 115582, https://doi.org/ 10.1016/j.desal.2022.115582.
- [9] G. Dibrov, G. Kagramanov, V. Sudin, E. Grushevenko, A. Yushkin, A. Volkov, Influence of sodium hypochlorite treatment on pore size distribution of polysulfone/polyvinylpyrrolidone membranes, Membranes 10 (11) (2020) 356, https://doi.org/10.3390/membranes10110356.
- [10] J. Ding, S. Wang, P. Xie, Y. Zou, Y. Wan, Y. Chen, M.R. Wiesner, Chemical cleaning of algae-fouled ultrafiltration (UF) membrane by sodium hypochlorite (NaClO): characterization of membrane and formation of halogenated by-products, J. Membr. Sci. 598 (2020) 117662, https://doi.org/10.1016/j. memsci.2019.117662.
- [11] Y. Kourde-Hanafi, P. Loulergue, A. Szymczyk, B. Van der Bruggen, M. Nachtnebel, M. Rabiller-Baudry, J.-L. Audic, P. Pölt, K. Baddari, Influence of PVP content on degradation of PES/PVP membranes: insights from characterization of membranes with controlled composition, J. Membr. Sci. 533 (2017) 261–269, https://doi.org/10.1016/j.memsci.2017.03.050.
- [12] K. Li, Q. Su, S. Li, G. Wen, T. Huang, Aging of PVDF and PES ultrafiltration membranes by sodium hypochlorite: effect of solution pH, J. Environ. Sci. (China) 104 (2021) 444–455, https://doi.org/10.1016/j.jes.2020.12.020.
- [13] B. Malczewska, A. Zak, Structural changes and operational deterioration of the Uf Polyethersulfone (pes) membrane due to chemical cleaning, Sci. Rep. 9 (1) (2019) 422, https://doi.org/10.1038/s41598-018-36697-2.
- [14] M. Chen, R. Shang, P.M. Sberna, M.W.J. Luiten-Olieman, L.C. Rietveld, S.G. J. Heijman, Highly permeable silicon carbide-alumina ultrafiltration membranes for oil-in-water filtration produced with low-pressure chemical vapor deposition, Sep. Purif. Technol. 253 (2020) 117496, https://doi.org/10.1016/j.seppur.2020.117496.
- [15] C. Li, W. Sun, Z. Lu, X. Ao, S. Li, Ceramic nanocomposite membranes and membrane fouling: a review, Water Res. 175 (2020) 115674, https://doi.org/ 10.1016/j.watres.2020.115674.
- [16] C. Guizard, G. Rios, Chapter 12 transport and fouling phenomena in liquid phase separation with inorganic and hybrid membranes, in: A.J. Burggraaf, L. Cot (Eds.), Membrane Science and Technology, Elsevier, 1996, pp. 569–618, https://doi.org/ 10.1016/S0927-5193(96)80015-5.
- [17] A. Szymczyk, P. Fievet, Ion transport through nanofiltration membranes: the steric, electric and dielectric exclusion model, Desalination 200 (1–3) (2006) 122–124, https://doi.org/10.1016/j.desal.2006.03.266.
- [18] S.S. Wadekar, R.D. Vidic, Influence of active layer on separation potentials of nanofiltration membranes for inorganic ions, Environ. Sci. Technol. 51 (10) (2017) 5658–5665, https://doi.org/10.1021/acs.est.6b05973.
- [19] J.Y. Chong, R. Wang, From micro to nano: polyamide thin film on microfiltration ceramic tubular membranes for nanofiltration, J. Membr. Sci. 587 (2019) 117161, https://doi.org/10.1016/j.memsci.2019.06.001.
- [20] P. Chen, X. Ma, Z. Zhong, F. Zhang, W. Xing, Y. Fan, Performance of ceramic nanofiltration membrane for desalination of dye solutions containing NaCl and Na2SO4, Desalination 404 (2017) 102–111, https://doi.org/10.1016/j. desal.2016.11.014.
- [21] M. Cha, C. Boo, C. Park, Simultaneous retention of organic and inorganic contaminants by a ceramic nanofiltration membrane for the treatment of semiconductor wastewater, Process. Saf. Environ. Prot. 159 (2022) 525–533, https://doi.org/10.1016/j.psep.2022.01.032.

- [22] T. Van Gestel, C. Vandecasteele, A. Buekenhoudt, C. Dotremont, J. Luyten, R. Leysen, B. Van der Bruggen, G. Maes, Salt retention in nanofiltration with multilayer ceramic TiO2 membranes, J. Membr. Sci. 209 (2) (2002) 379–389, https://doi.org/10.1016/S0376-7388(02)00311-3.
- [23] F. Li, Y. Yang, Y. Fan, W. Xing, Y. Wang, Modification of ceramic membranes for pore structure tailoring: the atomic layer deposition route, J. Membr. Sci. 397-398 (2012) 17–23, https://doi.org/10.1016/j.memsci.2012.01.005.
- [24] R. Shang, A. Goulas, C.Y. Tang, X. de Frias Serra, L.C. Rietveld, S.G.J. Heijman, Atmospheric pressure atomic layer deposition for tight ceramic nanofiltration membranes: synthesis and application in water purification, J. Membr. Sci. 528 (2017) 163–170, https://doi.org/10.1016/j.memsci.2017.01.023.
- [25] X. Zhou, Y.-Y. Zhao, S.-R. Kim, M. Elimelech, S. Hu, J.-H. Kim, Controlled TiO2 growth on reverse osmosis and nanofiltration membranes by atomic layer deposition: mechanisms and potential applications, Environ. Sci. Technol. 52 (24) (2018) 14311–14320, https://doi.org/10.1021/acs.est.8b03967.
- [26] E. Eray, V.M. Candelario, V. Boffa, H. Safafar, D.N. Østedgaard-Munck, N. Zahrtmann, H. Kadrispahic, M.K. Jørgensen, A roadmap for the development and applications of silicon carbide membranes for liquid filtration: recent advancements, challenges, and perspectives, Chem. Eng. J. 414 (2021) 128826, https://doi.org/10.1016/j.cej.2021.128826.
- [27] D. Hotza, M. Di Luccio, M. Wilhelm, Y. Iwamoto, S. Bernard, J.C. Diniz da Costa, Silicon carbide filters and porous membranes: a review of processing, properties, performance and application, J. Membr. Sci. 610 (2020) 118193, https://doi.org/ 10.1016/j.memsci.2020.118193.
- [28] M. Chen, S.G.J. Heijman, M.W.J. Luiten-Olieman, L.C. Rietveld, Oil-in-water emulsion separation: fouling of alumina membranes with and without a silicon carbide deposition in constant flux filtration mode, Water Res. 216 (2022) 118267, https://doi.org/10.1016/j.watres.2022.118267.
- [29] B. Hofs, J. Ogier, D. Vries, E.F. Beerendonk, E.R. Cornelissen, Comparison of ceramic and polymeric membrane permeability and fouling using surface water, Sep. Purif. Technol. 79 (3) (2011) 365–374, https://doi.org/10.1016/j. seppur.2011.03.025.
- [30] A. Jan, M. Chen, M. Nijboer, M.W.J. Luiten-Olieman, L.C. Rietveld, S.G.J. Heijman, Effect of long-term sodium hypochlorite cleaning on silicon carbide ultrafiltration membranes prepared via low-pressure chemical vapor deposition, Membranes 14 (1) (2024) 22, https://doi.org/10.3390/membranes14010022.
- [31] G. Qin, A. Jan, Q. An, H. Zhou, L.C. Rietveld, S.G.J. Heijman, Chemical vapor deposition of silicon carbide on alumina ultrafiltration membranes for filtration of microemulsions, Desalination 582 (2024) 117655, https://doi.org/10.1016/j. desal.2024.117655.
- [32] B. Morana, G. Pandraud, J.F. Creemer, P.M. Sarro, Characterization of LPCVD amorphous silicon carbide (a-SiC) as material for electron transparent windows, Mater. Chem. Phys. 139 (2) (2013) 654–662, https://doi.org/10.1016/j.matchemphys.2013.02.013.
- [33] E.W. Washburn, The dynamics of capillary flow, Phys. Rev. 17 (3) (1921) 273, https://doi.org/10.1103/PhysRev.17.273.
- [34] Y. Zhang, G. Ye, Z. Yang, Pore size dependent connectivity and ionic transport in saturated cementitious materials, Constr. Build. Mater. 238 (2020) 117680, https://doi.org/10.1016/j.conbuildmat.2019.117680.
- [35] C. Hoffmann, B. Reinhardt, D. Enke, S. Kaskel, Inverse silicon carbide replica of porous glasses, Microporous Mesoporous Mater. 184 (2014) 1–6, https://doi.org/ 10.1016/j.micromeso.2013.09.019.
- [36] R.J. Hunter, Zeta Potential in Colloid Science: Principles and Applications, Academic Press, 2013.
- [37] P.M. Biesheuvel, H. Verweij, Design of ceramic membrane supports: permeability, tensile strength and stress, J. Membr. Sci. 156 (1) (1999) 141–152, https://doi.org/ 10.1016/S0376-7388(98)00335-4.
- [38] M. Nijboer, A. Jan, M. Chen, K. Batenburg, J. Peper, T. Aarnink, F. Roozeboom, A. Kovalgin, A. Nijmeijer, M. Luiten-Olieman, Tuning Nanopores in tubular ceramic nanofiltration membranes with atmospheric-pressure atomic layer deposition: prospects for pressure-based in-line monitoring of pore narrowing, Separations 11 (1) (2024) 24, https://doi.org/10.3390/separations11010024.
- [39] J. Randon, A. Julbe, P. David, K. Jaafari, S. Elmaleh, Computer simulation of inorganic membrane morphology: 2. Effect of infiltration at the membrane support interface, J. Colloid Interface Sci. 161 (2) (1993) 384–388, https://doi.org/ 10.1006/jcis.1993.1481.
- [40] C.-F. Wang, D.-S. Tsai, Low pressure chemical vapor deposition of silicon carbide from dichlorosilane and acetylene, Mater. Chem. Phys. 63 (3) (2000) 196–201, https://doi.org/10.1016/S0254-0584(99)00207-2.
- [41] Y.S. Lin, A theoretical analysis on pore size change of porous ceramic membranes after modification, J. Membr. Sci. 79 (1) (1993) 55–64, https://doi.org/10.1016/ 0376-7388(93)85017-0
- [42] M.B. Tanis-Kanbur, R.I. Peinador, J.I. Calvo, A. Hernández, J.W. Chew, Porosimetric membrane characterization techniques: a review, J. Membr. Sci. 619 (2021) 118750, https://doi.org/10.1016/j.memsci.2020.118750.
- [43] S. Bhattacharjee, DLS and zeta potential what they are and what they are not? J. Control. Release 235 (2016) 337–351, https://doi.org/10.1016/j.iconrel.2016.06.017.
- [44] E. Eray, V. Boffa, M.K. Jørgensen, G. Magnacca, V.M. Candelario, Enhanced fabrication of silicon carbide membranes for wastewater treatment: from laboratory to industrial scale, J. Membr. Sci. 606 (2020) 118080, https://doi.org/ 10.1016/j.memsci.2020.118080.
- [45] I. Caltran, L.C. Rietveld, H.L. Shorney-Darby, S.G.J. Heijman, Separating NOM from salts in ion exchange brine with ceramic nanofiltration, Water Res. 179 (2020) 115894, https://doi.org/10.1016/j.watres.2020.115894.

- [46] J.V. Nicolini, C.P. Borges, H.C. Ferraz, Selective rejection of ions and correlation with surface properties of nanofiltration membranes, Sep. Purif. Technol. 171 (2016) 238–247, https://doi.org/10.1016/j.seppur.2016.07.042.
- [47] J.M. Skluzacek, M.I. Tejedor, M.A. Anderson, Influence of membrane support structure on the efficiency of an iron-modified silica nanofiltration membrane, J. Porous. Mater. 15 (2008) 303–309, https://doi.org/10.1007/s10934-006-9083-1
- [48] S.S. Wadekar, R.D. Vidic, Comparison of ceramic and polymeric nanofiltration membranes for treatment of abandoned coal mine drainage, Desalination 440 (2018) 135–145, https://doi.org/10.1016/j.desal.2018.01.008.
- [49] R.J. Gross, J. Osterle, Membrane transport characteristics of ultrafine capillaries, J. Chem. Phys. 49 (1) (1968) 228–234, https://doi.org/10.1063/1.1669814.
- [50] H.K. Lonsdale, W. Pusch, A. Walch, Donnan-membrane effects in hyperfiltration of ternary systems, J. Chem. Soc., Faraday Trans. 1 71 (1975) 501–514, https://doi. org/10.1039/F19757100501.
- [51] E.R. Nightingale Jr., Phenomenological theory of ion solvation. Effective radii of hydrated ions, J. Phys. Chem. 63 (9) (1959) 1381–1387, https://doi.org/10.1021/ j150579a011.